Numerical Modelling and Experimental Verification of New Observations of the Two Phases Interaction in a Vertical and Inclined Closed Wickless Heat Pipe

Alaa A. B. Temimy[1]   **Adnan A. Abdulrasool[2]**

1) Training and Power Research Office, Ministry of Electricity, Baghdad, Iraq

dralaatemimy@yahoo.com

2)   Mechanical Engineering Department, Al-Mustansiriayah University, Baghdad, Iraq

adnan_ameer54@yahoo.com

Abstract

Heat pipes are one of the modern solutions for heat release from hot sources or for heat homogeneity in liquid or solid reservoirs. The interactions between the two phases of its working fluid are suggested classically by researchers and still not discovered deeply. In this study about 480 experimental and numerical tests are carried out to confirm the previous published observation of spatial flow patterns of the two phases inside a wickless copper Thermosyphon Heat Pipe THP partially filled with water. Numerical results are gotten from a three dimensional transient Computational Fluid Dynamics 3DCFD numerical solution. Different factors are included into 3DCFD model to reach reality in results and suffering from complex calculation procedures and increase simulation running time. The high agreement percentages between the experimental and 3DCFD for the temperatures distribution profile and magnitudes confirm the 3DCFD results. 3DCFD solution contours of steam volume fractions SVF show that both phases flow in a 3D spatial, non-steady and non-continues flow streams. Both phases suffering phase change and heat transfer from each to other during flow up (steam) and flow down (condensate). Thermal performance increase about (+ve. (10%)) due to inclination from vertical to 60º then falling to (-ve. (15%)) at 15º (for filling ratio 50% and heat supplied 200W). that's because inclination lead the complex spatial flow to be a uniform circulation flow, hence it's lead to non-homogeneity in evaporation and condensation processes and finally result in reduction of thermal performance.

Keywords: Two-phase thermosyphone, Heat pipe, Performance, Experimental, Computational fluid dynamics (CFD), Flow pattern modelling, Inclination, Evaporation, Condensation, Water.

Abbreviations

Symbol	Description and Units
C	Coefficient of surface curvature (-)
$C_{v,l}$	Specific heat (kJ/kg K)
E	Energy (kJ)
g	Gravitational acceleration (m/sec^2)
HP	Heat Pipe
I	Unit tensor
P	Pressure (pa)
Q	Supplied heat (W)
R_{th}	Thermal resistance (K/W)
S_E	Energy source parameter
S_m	Phase change (mass source) term used to estimate the mass transfer from one phase to another during evaporation and condensation.
$T_{evap.avg.}$	Average temperature of evaporator section (K)
$T_{cond.avg.}$	Average temperature of condenser section (K)
THP	Thermosyphon Heat Pipe
t	Time (sec)
V	Velocity vector
α_l	Liquid volume fraction (-)

α_v	Vapor volume fraction (-)
μ	Dynamic viscosity (N sec/m^2)
ρ	Density (kg/m^3)
σ	Surface tension (N/m)

1. Introduction

One of the modern devices for high rate of heat transfer are Heat pipes [1]. They are depending on passive techniques for heat transfer of standalone continues cycles of evaporation and condensation [2]. Where heat transferred to the working media at evaporator section leads the liquid to evaporate and travel to condenser section by buoyancy forces to release heat and condensate, then return to the evaporator by gravity forces. Also they are one of the modern solutions for high rates of heat transfer due to its simplicity , low manufacturing cost and no-maintenance required [3]. Due to the above mentioned advantages, heat pipes are used in a very wide range of applications [4], [5] such as cooling of electronic devices [6]–[10], solar applications [11], solar heat storages [12] , cooling of wind towers [13],and space applications [14], [15], [16].

Thermosyphon or Wickless Heat Pipes THP from its early discovered in 1960th[3], divided normally into three working sections: Evaporator section, Adiabatic section and Condenser section as shown in Fig. 1 [3]. The working fluid (water in our study) absorb heat from evaporator wall and evaporate (as a steam) then move due buoyancy forces towards condenser section through adiabatic section. This movement suggested classically being in the core of the heat pipe. In condenser section, the steam releases its heat to condenser wall and condensate then return to the evaporator section by gravity forces. This return suggested classically being at the wall of the heat pipe.

Many engineering tools and applications has been developed rapidly when using Computational Fluid Dynamic CFD numerical solutions to predict their actual or simulated working behavior and data [17]–[19]. Also the rocket development of high speed calculating processors and capabilities of computers lead CFD programmers to add more and more calculating parameters to reach reality in results with a minimum percentages of errors [18], i.e. increase CFD solutions accuracy, efficiency, universality and flexibility. Finally minimize the experimental tests needed for tools and devices development, and experimental work results data used to validate and confirm CFD results.
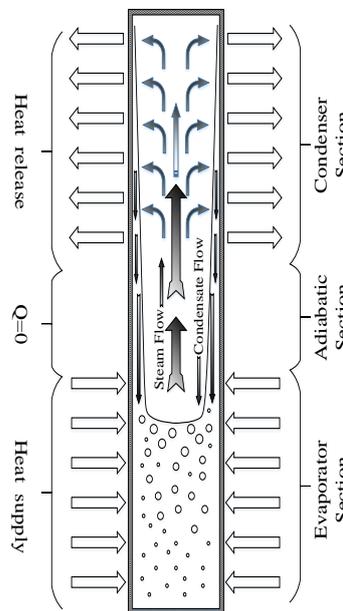
Figure (1): Classical schematic diagram of THP [3]

2. Literature survey

Many review articles about HPs has been printed and published and all of them assuming the same classical flow pattern of steam and condensate [2]–[5], [20], [21] that shown in Fig 1. Some attempts are made by researchers to visualize heat transferred and temperature distribution such as R. Boukhanouf et.al. in 2006 [22] visualize the distribution of heat on a flat evaporator of HP using IR

thermal imaging camera and compare the heat distribution with a solid copper flat plate . Nemec et.al in 2010 [23] visualize heat transfer from the HP walls using a thermos-camera and compare temperature distribution along HP with various types of capillary structures. During the last 10 years, researchers has start to use the benefit of high performance computers to solve and monitor the complex fluid flow problems, such as Wang and Jung Chang in 2012 [24], they use a 3-dimensional 3D Ice Pak software to simulate the flow behavior over a single flat and 3 imbedded HP used to cooling a VGA card and validate the results with experimental tests with error of 5%. A. Eidan et.al. in 2016 [25] study numerically and experimentally THP performance for 6 different working fluid at a range of filling ratios and supplied heat. The numerical solution carried with FORTRAN code, neglecting phase change and velocity profiles with a constant classic phase's distribution. The agreement between numerical and experimental results less than 10%. H. Jouhara et.al. in 2016 [26] use ANSYS/Fluent software to simulate the boiling regime of water and R134a refrigerant near the evaporator wall of THP at low power supplied (geyser boiling). Their results show that the CFD can highly simulate the phase change and heat transfer of working fluids. Peterson G. et.al. in 2014 [2], show that the inclination from vertical (90º) increase thermal performance till inclination of (~70º) then the performance fall rapidly. In addition, this behavior is related to the Bond No. BO of the working fluid (i.e the relation between gravitational and surface tension forces). Alammar A. et.al in 2016 [27] study experimentally and numerically using ANSYS/Fluent software the effect of filling ratio and inclination angle on THP thermal performance. They found that at low filling ratio and low inclination angle there is a significant increase in evaporator temperatures. In addition, the maximum deviation between CFD and experimental results for temperatures distribution is 4.2% S. Aswath et.al. in 2017 [11] study the difference in THP performance for solar heating numerically using ANSYS for the same geometry with water and ammonia as working fluid. The CFD results show that ammonia creating a better temperature distribution along THP than water. A. Temimy et.al. in 2019 [28], set up a CFD model configurations using ANSYS R19 / Fluent software based on Volume Of Fluid VOF model to simulate the temperatures distribution , two-phases interactions and flow behaviors of vertical THP partially filled with water at various heat supply and filling ratios. The simulation results show that the two phases move up-ward (steam) and downward (condensate) at a complex spatial flow behavior compared to the classical suggestion of the flow for the steam to be at the core and the condensate at the wall.

Two goals are suggested for this study, first one is to validate the 3D CFD results [28]experimentally based on temperatures distribution results along the THP in transient and steady state conditions at various filling ratios and heat supply. Second, one is to simulate and study the effect of inclination angles on thermal performance of THP.

Governing equations

The governing mathematical equations used in the CFD calculations to get transient and steady states thermal parameters, velocities and volume fractions of each phase are as follows [29]–[31]:

2.1. Continuity equation

Since the volume fractions VR of each phase keep change during operation of THP. So that to find out the VOF equations of each phase of the working fluid at each time interval, the equation of continuity has the following form based on the coincide conservation of masses of both phases:

$$\nabla \cdot (\rho V) = -\frac{\partial \rho}{\partial t} \qquad (1)$$

Equation 1 initially solved to track the change in volume fractions of primary phase (v-vapor). Then eqn. 2 can track the change in volume fractions of the other phase (l-liquid) as follow:

$$\nabla \cdot (\propto_l \rho_l V) = -\frac{\partial}{\partial t}(\propto_l \rho_l) + S_m \qquad (2)$$

To get the accurate solution for primary phase volume fractions, the following eqn. should have satisfied:

$$\sum_{v=1}^{n} \propto_v = 1 \qquad (3)$$

A mixture of the phase's v and l exists when the cell is not wholly full with primary phase (v) or with the secondary phase (l). So that, the mixture density is calculated as the averaged density volume fraction as follow:

$$\rho = \propto_l \rho_l + (1 - \propto_l)\rho_v \tag{4}$$

2.2. Momentum equation

In VOF model the main forces acting on the fluid phases are surface tension, pressure, gravitational, and friction. To calculate the effect of surface tension along the interface of two phases, the parameter continuum surface force (CSF) has been added to the 3D momentum equation

$$F_{CSF} = 2\sigma \frac{\propto_l \rho_l C_v \nabla \alpha_v + \propto_v \rho_v C_l \nabla \alpha_l}{\rho_l + \rho_v} \tag{5}$$

The momentum equation will be as follows when considering the FCSF forces into VOF model:

$$\frac{\partial}{\partial t}(\rho V) + \nabla \cdot (\rho V V^T) = \rho g - \nabla p + \nabla \cdot \left[\mu(\nabla V + (\nabla V)^T) - \frac{2}{3}\mu(\nabla \cdot V)I \right] + F_{CSF} \tag{6}$$

The dynamic viscosity μ calculated as follow:

$$\mu = \propto_l \mu_l + (1 - \propto_l)\mu_v \tag{7}$$

2.3. Energy equation

The energy equation has the following form for the VOF model:

$$\frac{\partial}{\partial t}(\rho E) + \nabla \cdot (\rho E V) = \nabla \cdot (k\nabla T) + \nabla \cdot (pV) + S_E \tag{8}$$

Where energy source parameter SE is used to compute the heat transfer during condensation and evaporation.

The equivalent thermal conductivity k calculated as follow:

$$k = \propto_l k_l + (1 - \propto_l)k_v \tag{9}$$

Also the mass averaged calculation for energy E are applied as follow:

$$E = \frac{\propto_l \rho_l E_l + \propto_v \rho_v E_v}{\propto_l \rho_l + \propto_v \rho_v} \tag{10}$$

Finally, energy terms for each phase based on specific heats and temperatures will be calculated as follows:

$$E_l = C_{v,l}(T - T_{sat}) \tag{11}$$

$$E_v = C_{v,v}(T - T_{sat}) \tag{12}$$

2.4. Thermal resistance

The thermal performance of THP is usually represented in different ways that used to compare different configurations for one application [1], [3], [5], [21], [32]. One of these is the thermal resistance of THP that represent the ratio of the difference between averaged temperatures of evaporator and condenser sections to the supplied heat as given in (13) bellow

$$R_{th} = \frac{T_{evap.avg.} - T_{cond.avg.}}{Q} \tag{13}$$

So that, the lower thermal resistance THP is the best between many configurations for the same heat supplied.

3. **Model geometry and dimensions**

The THP dimensions and working conditions for the CFD model and test rig are selected based on common library testing dimensions and working conditions [25]–[27], [33]–[36], [37]–[39][40]–[43], and they are as follow:

- a- Material: copper
- b- Working fluid: water
- c- Pipe OD/ID: 19.05mm / 17.4 mm
- d- Length: 600mm (Evaporature:250mm, Adiabatic:150mm, Condenser: 200mm)
- e- Jacketed condenser ID: 50 mm (along condenser section)
- f- Filling ratios: 40%, 50%, 60%, 70% (of evaporator volume)
- g- Heat supply: 50, 75, 100, 150, 200 Watt
- h- Inclination angles: 15°,30°,45°,60°,75°,90° with horizontal
- i- Cooling water flow rate: 3 lit./min

The model geometry and its dimensions is shown in Fig. 2 below.
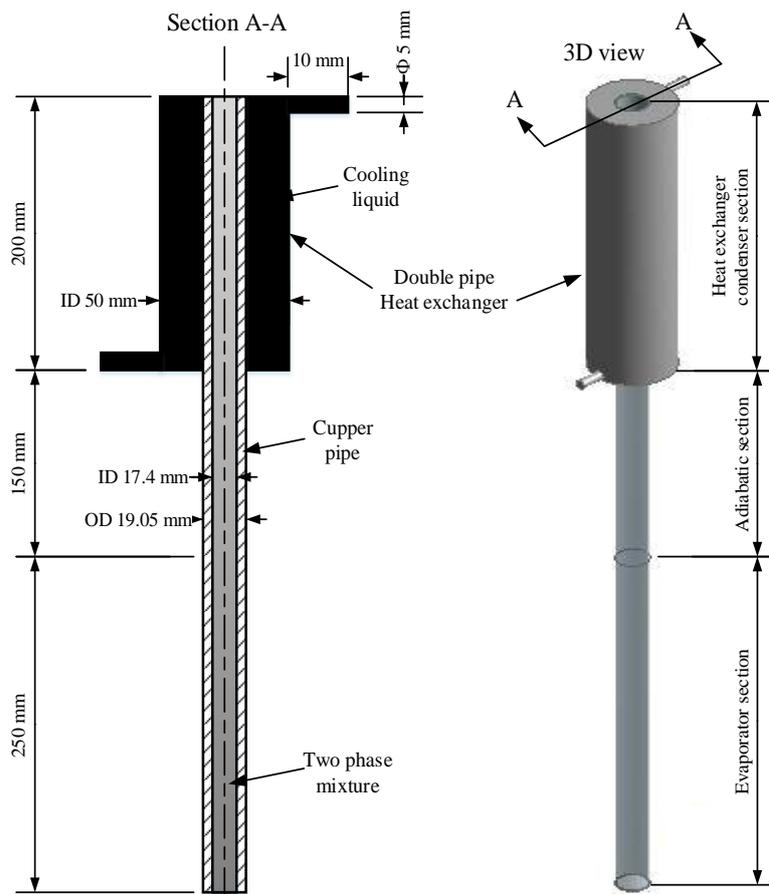
Figure (2): Model geometry and dimensions

4. **CFD model setup**

ANSYS / Fluent R19 software used to get the 3D CFD solutions for the present experimental work [28]. The model arranged and it dimensions are set as shown in Fig. 2 above including water jacket heat exchanger using Fluent – Geometry software. A mesh with about 2 Million nodes are arranged as

shown in Fig. 3. Inflation module has been used to concentrate the mesh nodes near the inner and outer pipe surfaces to capture phase change and heat transfer in boundary layers. Mesh non-independency procedure with error less than 1% are used till this 2M nodes are select as a proper mesh.

The 3D CFD solution set as transient and pressure based solution and gravitational acceleration activated with (-9.81N/sec2) in Y direction. In modules window, a multiphase Euler-Euler solution procedure with 2-phases are selected [30], vapor (steam) as primary phase and liquid (water) as secondary phase. VOF model with explicit volume fractions parameters and local phase discretization with value of (1) are selected [29], [31]. Water and copper are selected from the built-in materials library of Fluent.

Top view
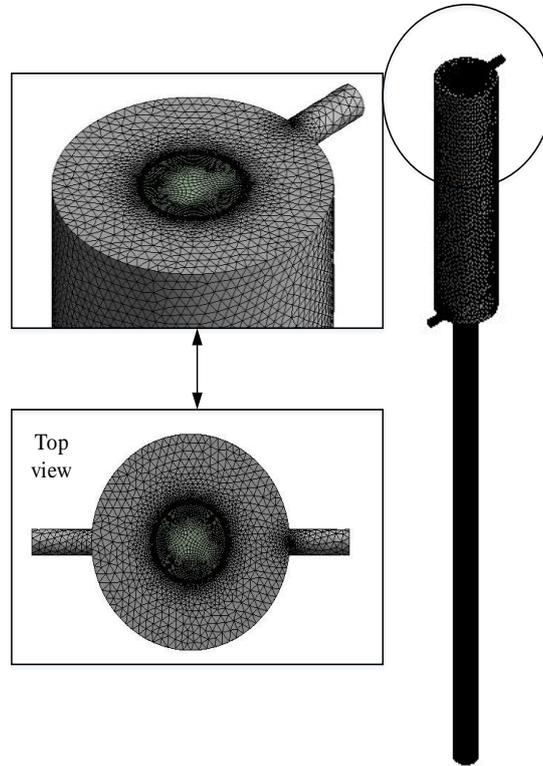
Figure (3): 3D CFD Model Mesh, about 2 Million nodes

Vapor set as primary phase and liquid set as secondary phase. All the model are set initially at 25Cº. Supplied heat flux set at outer surface of the evaporator. Zero heat flux set at adiabatic section outer surface i.e. insulated surface. Inlet cooling water flowrate set at 3lit./min. at constant temperature of 25Cº and the outlet set as atmosphere. All other surfaces are set thermally coupling. Adapting procedure used to set the filling ratio. Time step of 10-4 sec are set to insure that Courant number less than unity. Auto-save case and data file set at each 10 time steps i.e. each 0.01 sec to trace and monitor the phases interaction and the variations of other required parameters for study comparison and validation. When the heat absorbed by cooling water equal the heat supplied, then steady state condition was satisfied and stop the calculation for the case [28]. Time required to complete one run was about 50 hours, and number of time steps recorded of the case steady from start-up till steady state was about 12*106 time step, i.e the simulated time for the case study is about (10-4 sec* (12*106) time step)≈20 minutes.

5. Experimental work

The experimental part is used to validate the 3D CFD solution results and to verify the disagreement if any noticed. A test rig was built to get the experimental data for study cases based on model configuration and working parameters discussed previously. The test rig and its components definitions are shown in Fig.4 below.

1- THP
2- Injection valve
3- Suction valve
4- Vacuum motor
5- Vacuum gauge
6- Injection syringe (100) ml.
7- Flow meter
8- Cooling water control valve
9- Cooling water inlet
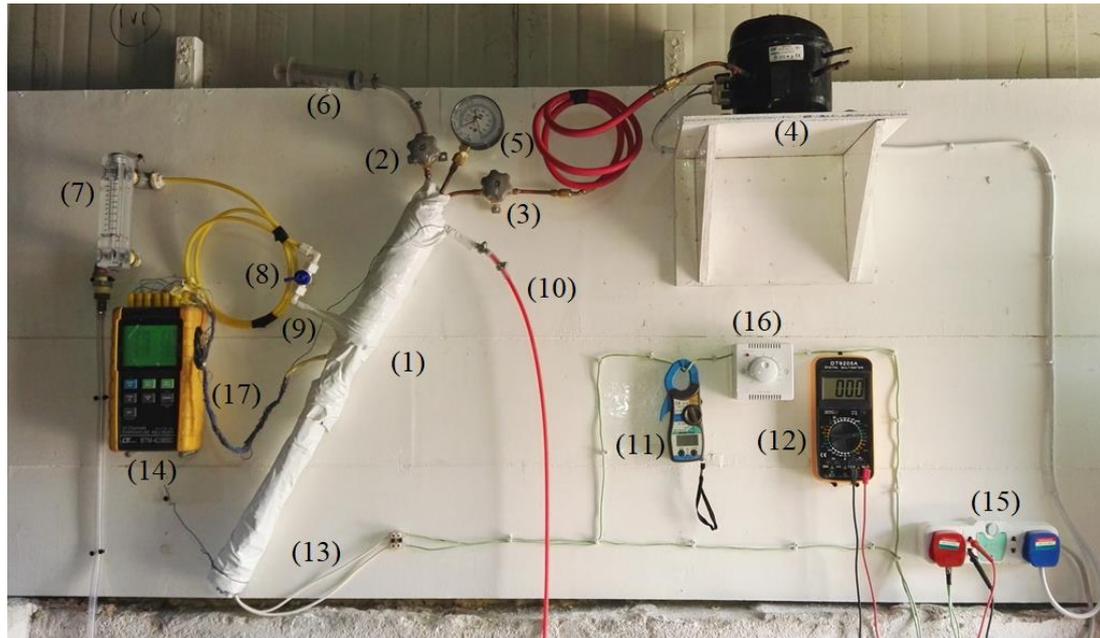
10- Cooling water outlet
11- Supply power current meter
12- Supply power voltmeter
13- Heating elements
14- Data logger + Memory card
15- Supply power
16- Variable resistance (Variac)
17- Thermocouples wires

Figure (4): Test rig arrangement and components

A copper THP was made and 11 type (k) thermocouples are attached to it to get temperatures distribution. Thermocouples arranged as follows: (1,2,3,4,5) at evaporator section; (5,6,7) at adiabatic section; (7,8,9) at condenser section; (10) cooling water inlet; (11) at cooling water outlet. Six longitudinal heating elements arranged and fitted around the evaporator section. To insure homogeneous heat flux supply to the evaporator section, a thermal clay was applied and fill the gaps between the heating elements. The THP and attached thermocouples are thermally insulated with one-inch thickness of glass wool and taped with insulated tape. All experimental instruments and devices are calibrated based on standard calibration procedure for each one.

6. Results and discussion

Fig.5 shows the temperature distribution contours using 3D CFD for vertical THP, 50% filling ratio, and 200W heat supply. Results confirm previous results given in [28] and used here as a case study.

In addition, the steam volume fraction contours at vertical center and cross sectional planes, gave the same look for the spatial non-homogenous flow patterns and steam-condensate inter-actions as shown in Fig.6 (a-n). Were the steam move up due-to buoyancy forces near the wall due its high temperature and low density of fluid in the boundary layer, and the condensate flow down due to gravitational forces near the wall due to condensation on the wall. When the phases face each other, the high momentum phase continue its flow and shift the other phase from its way. However, due to high shear stresses results from the interaction, both phases affect each other flow streams and lead to the spatial flow patterns of both.

Experimental data are gathered and calibrated based on calibration curves of the instruments and devices used in tests. Since we repeat each case three times, the average readings are used. The temperature distribution results of experimental tests confirm the 3D CFD results and they are plotted together as shown in Fig.7 (a-f) for filling ratio 50%. As shown in Fig.7 (a-f), both experimental tests and 3D CFD give the same temperature distribution profile along THP. But 3D CFD is with relatively higher temperatures. This behavior may be due experimental heat losses to the surroundings during experimental tests, so that the actual heat supplied and absorbed by cooling water is less than the supplied

power. While into 3D CFD simulation, the absorbed heat by cooling water is assumed equal to that of the supplied heat. The error deviation calculated for the temperature distribution for all tested cases was less than 10%.
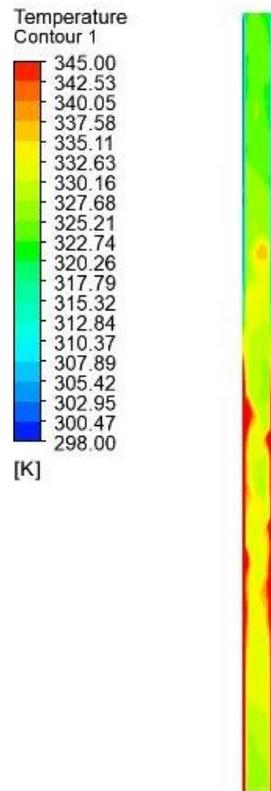
Figure (5): 3D CFD temperature distribution results sample
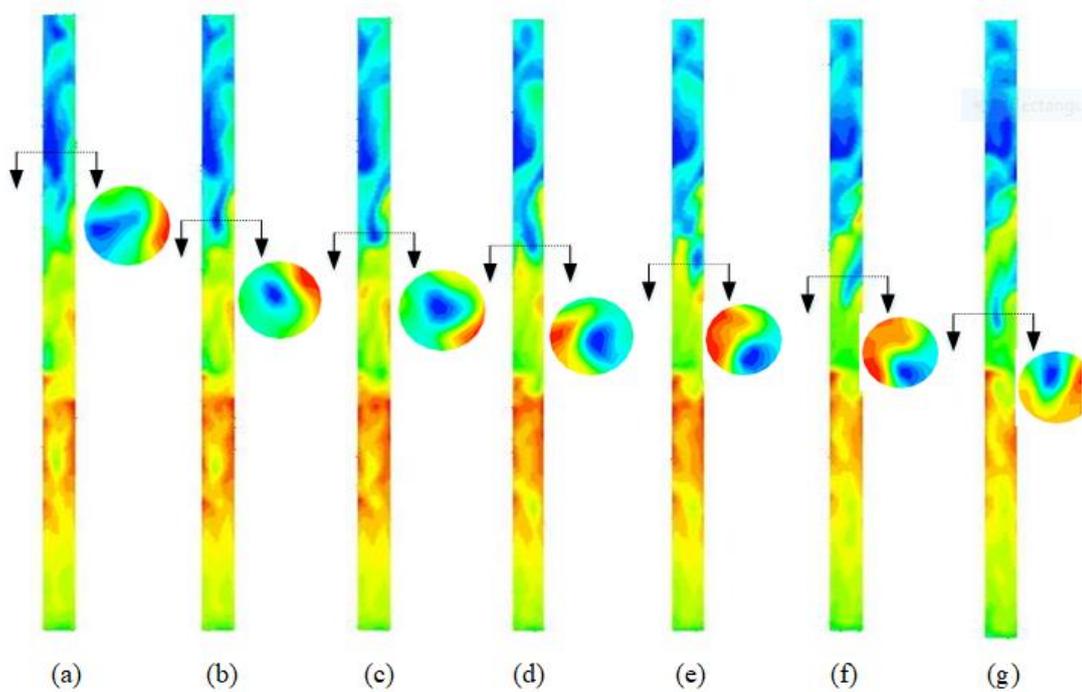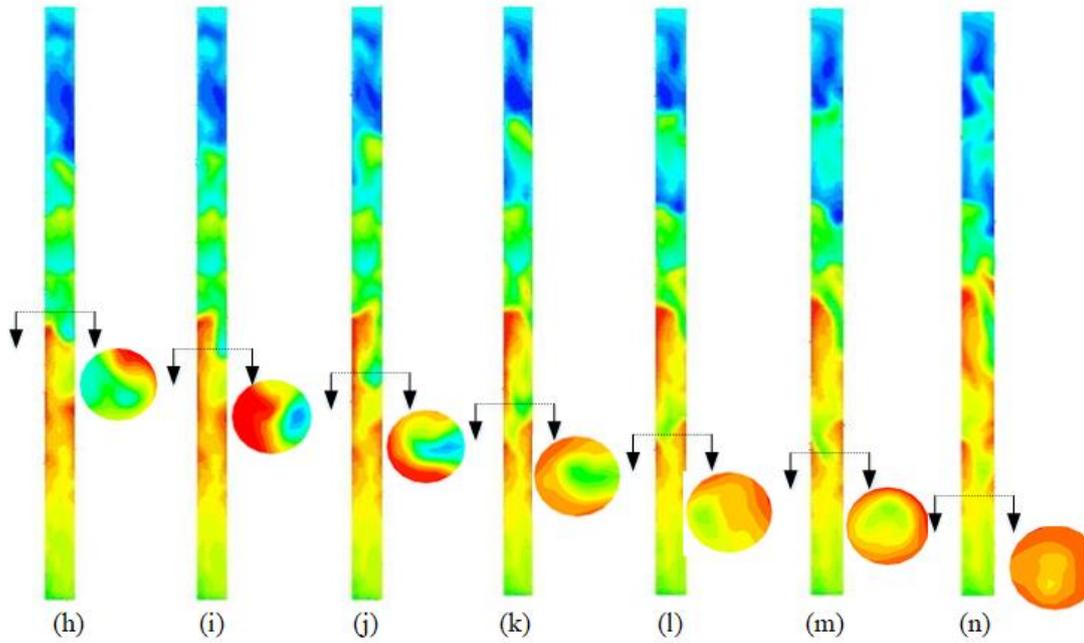
Figure (6 (a-n)): 3D CFD results for steam volume fractions flow patterns and two-phases inter-actions

(a) FR 50 % , 90º

(b) FR 50 % , 75º

(c) FR 50 % , 60º

(d) FR 50 % , 45º

(e) FR 50 % , 30º

(f) FR 50 % , 15º
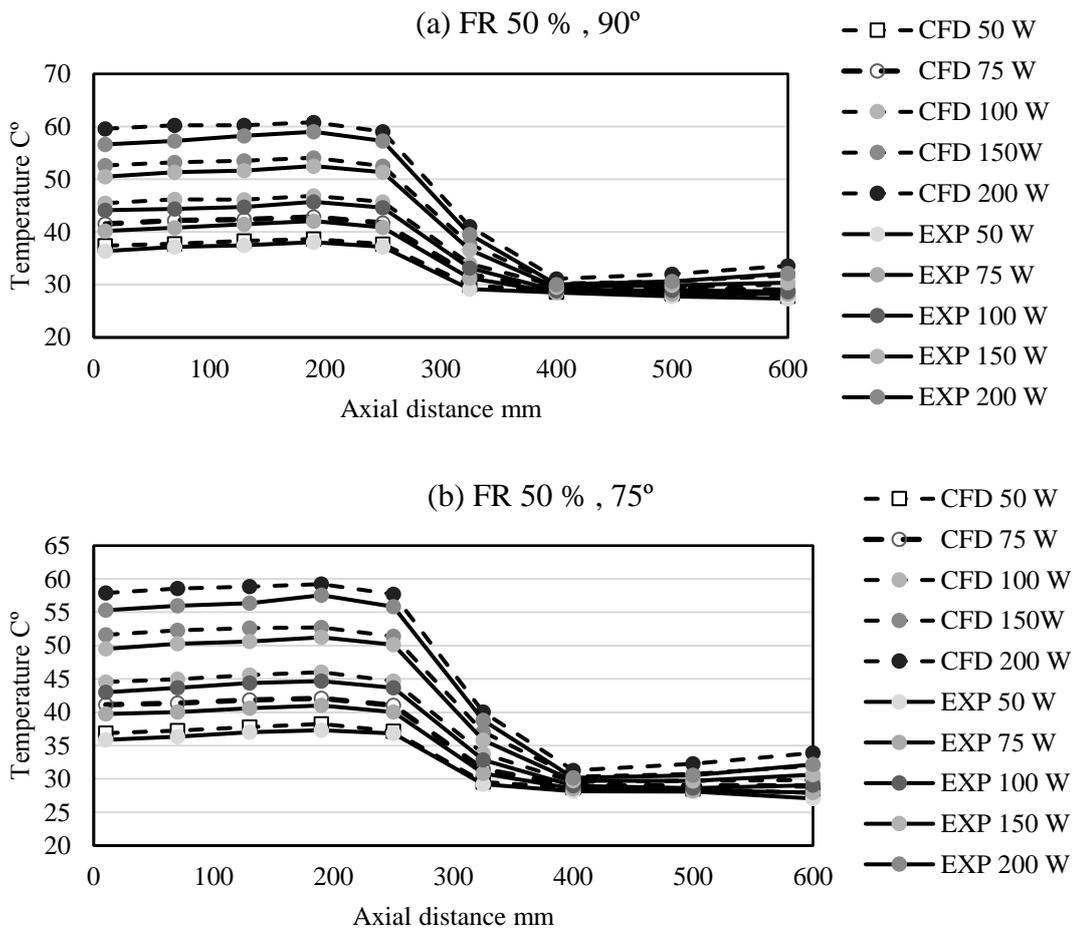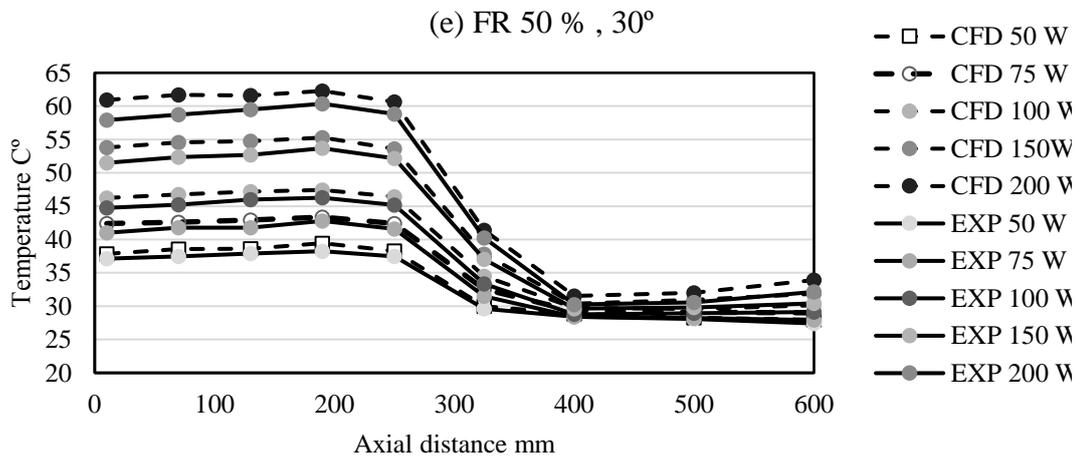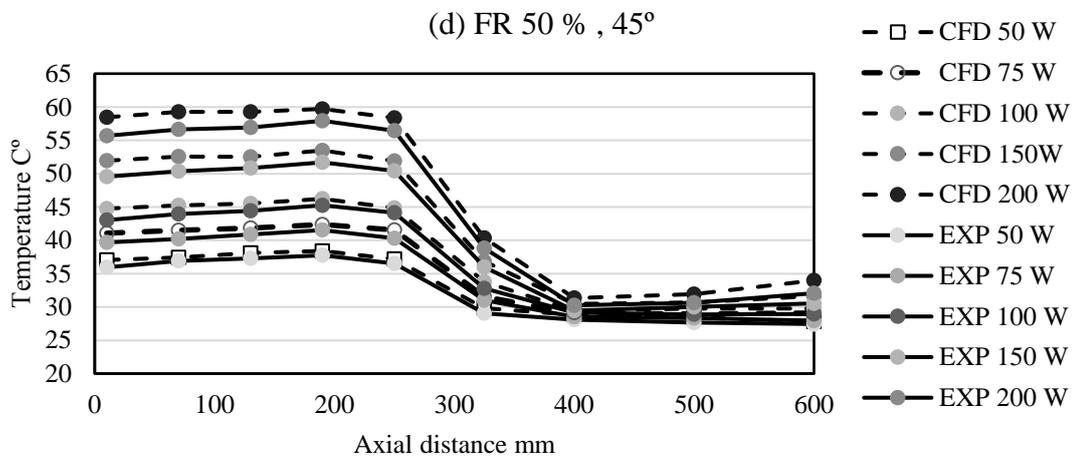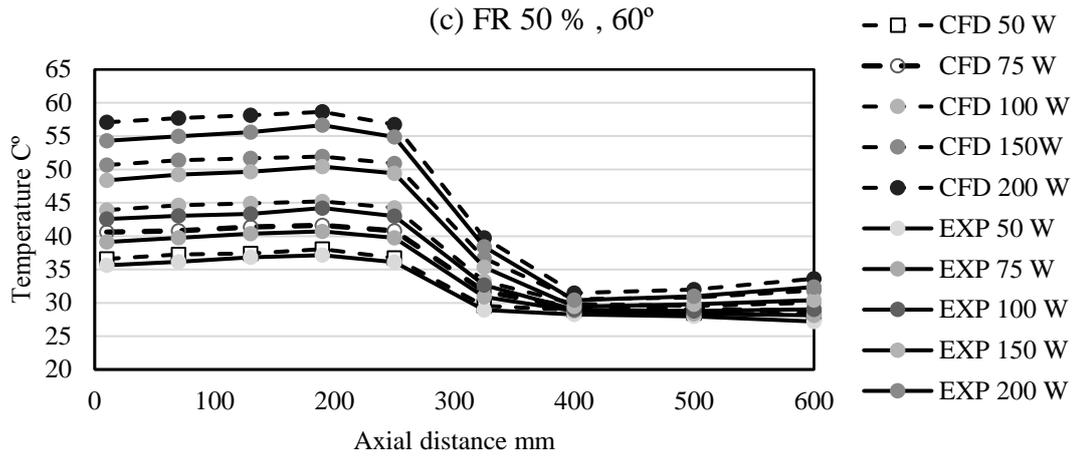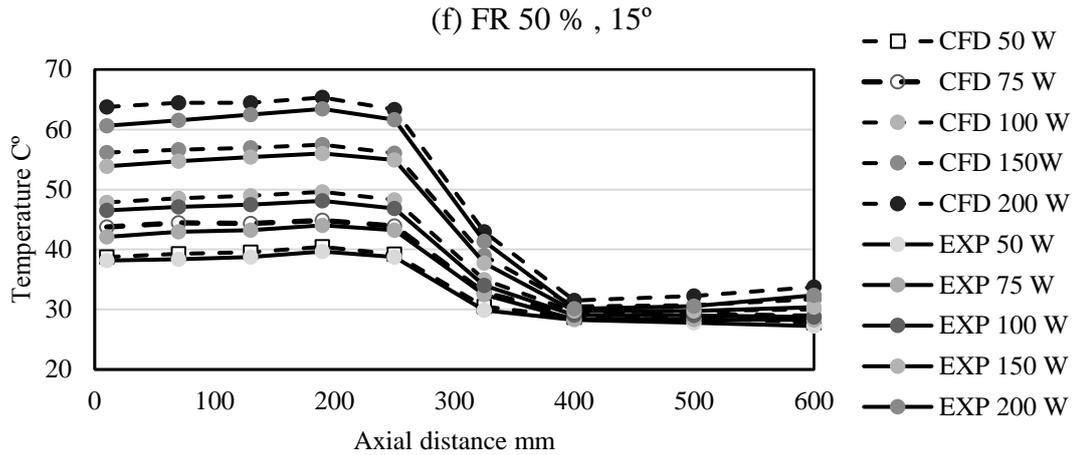
Figure (7(a-f)): Experimental and 3D CFD temperature distribution results sample

To study the effect of inclination angle on thermal performance or thermal resistance of THP see Figs.8,9,10 for filling ratio 50%. The lower thermal resistance position represents the high thermal performance. It's clear that thermal resistance decreased due to the increase in the supplied heat. This behavior is a known traditional behavior for the THP due to increasing of input heat with limited temperature difference between evaporator and condenser sections (see eqn.13). Also the thermal resistance of THP was decreased about 10% due-to inclination from 90º to 60º, but its raise up rapidly about (-15%) when THP go to semi-horizontal position at 15º,(this results confirm other researchers results [2], [3]). The inclination was suggested by the researchers will make a more stable circulation of the two-phases inside THP. However, the 3D CFD and experimental tests results gave a variable result for the effect of inclination. 3D CFD steam volume fractions contours of inclined THP clarify the reasons of this variable behavior as shown in Fig11 (a-f).
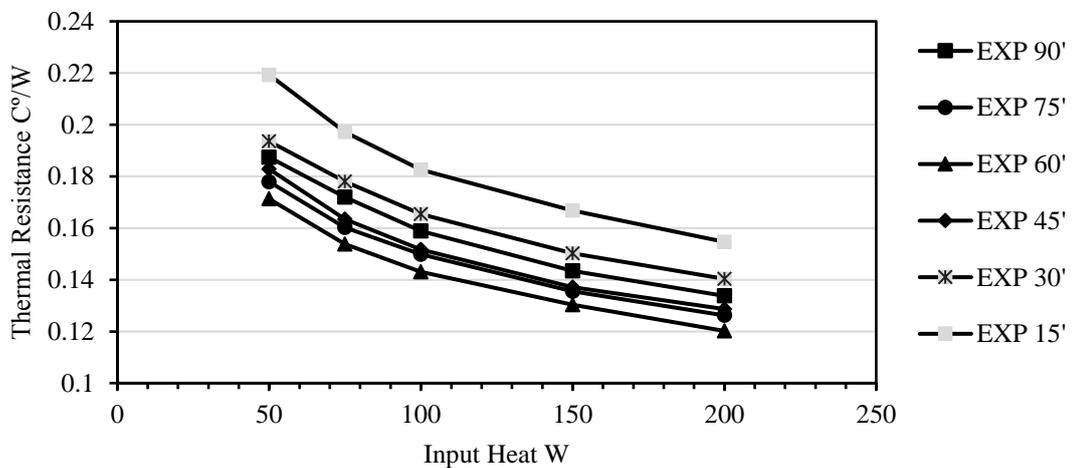
Figure (8): Experimental Thermal Resistance for filling ratio 50%
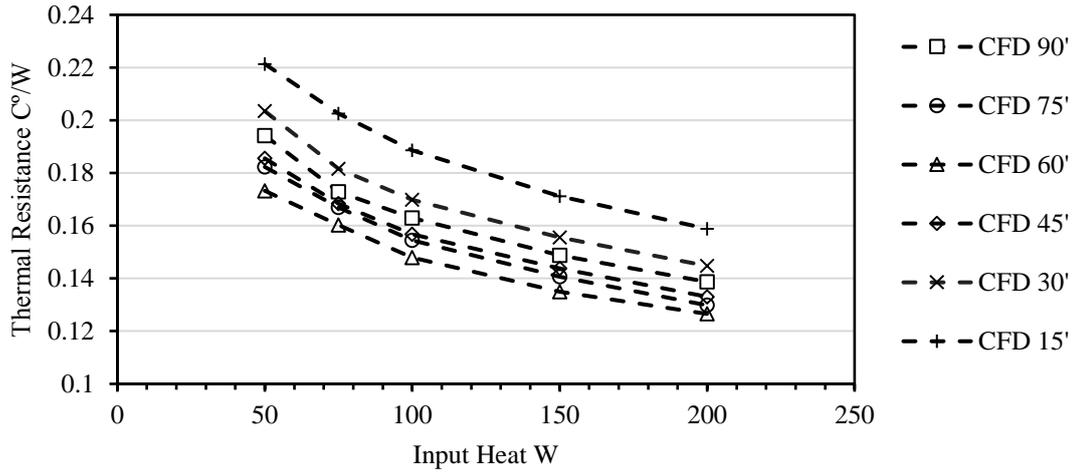
Figure (9): 3D CFD Thermal Resistance for filling ratio 50%
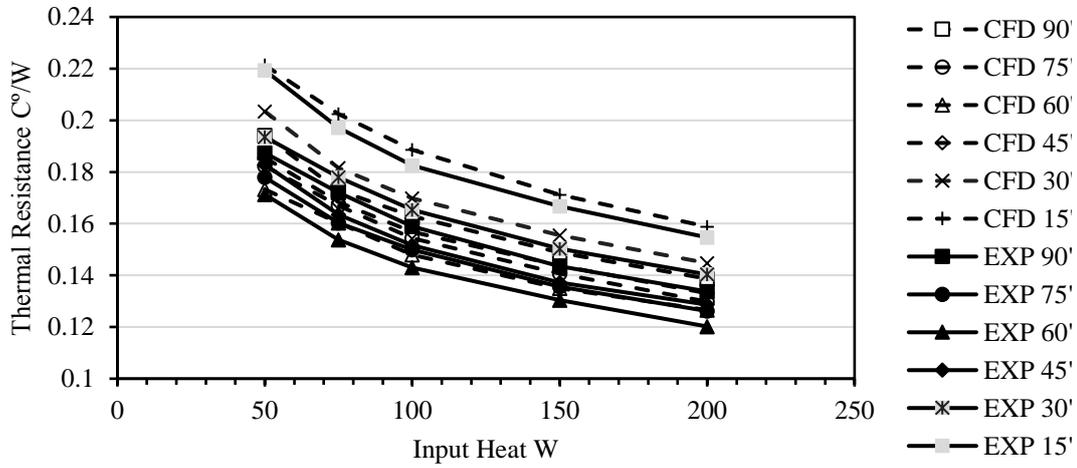
Figure (10): Experimental and 3D CFD Thermal Resistance for filling ratio 50%

(a)-90º   (b)-75º   (c)-60º

(d)-45º

(e)-30º

(f)-15°
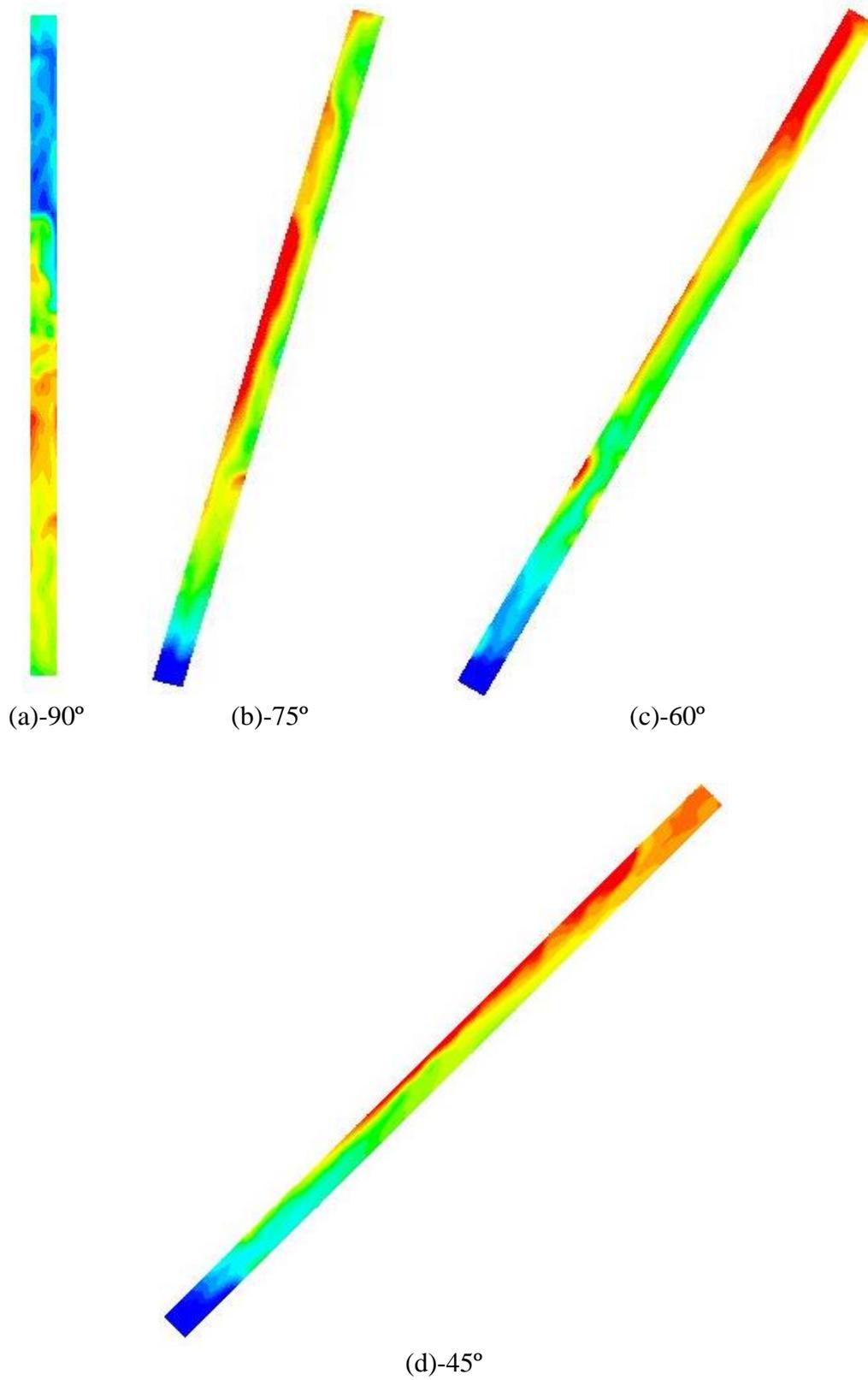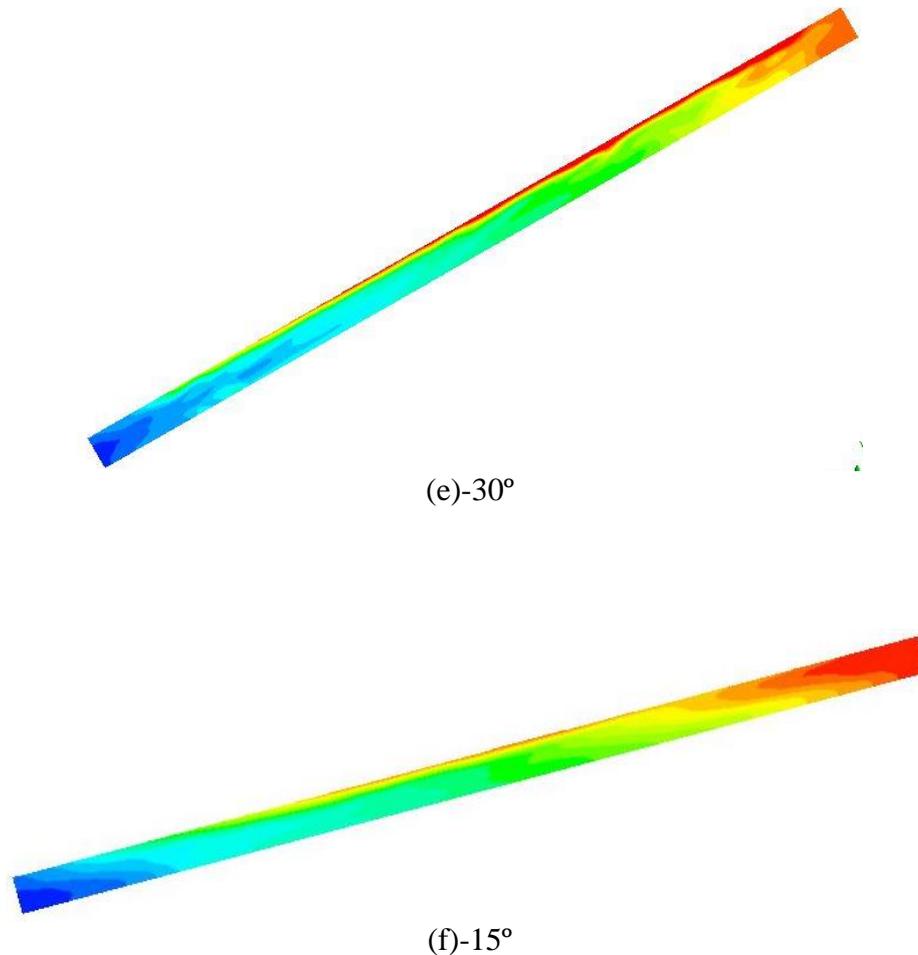
Figure (11(a-f)): Steam volume fraction contours at different inclination angles for filling ratio 50%

As shown in Fig.11 (a-f), as THP become more nearer to horizontal position, the circulation of the two-phases become more and more stable, i.e. generated steam flow near the upper surface from evaporator to the condenser, and condensate return from condenser to the evaporator at the lower surface. But this streams distribution lead to a non-homogeneity in evaporation and condensation processes. This is because evaporation occurs at a portion of evaporator surface, and condensation occurs at a portion of condenser surface. This lead to drop the evaporation and condensation processes efficiency and finally drop the thermal performance of THP due to farther inclination.

Conclusions

3D CFD Numerical solutions was a very good tool to predict and simulate variation of THP variables during transient and steady state conditions. The high agreement percentages between 3D CFD and experimental results can give an alternative to the experimental work, and make optimization of different configurations of THP easy and faster. Also 3D CFD simulation clarify the real reasons that leads to the drop in the thermal performance of THP due to inclination from vertical toward horizontal position. The simulation shows that due to inclination of THP the evaporation occurs at a portion of evaporator surface and condensation occurs at a portion of condenser surface, and lead finally to drop the efficiency of evaporation and condensation processes, hence lead to reduce the overall THP thermal performance.

Acknowledgement

CONFLICT OF INTERESTS.

There are no conflicts of interest

References

[1]S. Lips, V. Sartre, F. Lefèvre, S. Khandekar, and J. Bonjour, "Overview of heat pipe studies during the period 2010-2015," 2017.

[2]D. A. Reay, P. A. Kew, and R. J. McGlen, *Heat pipes Theory, Design and Applications*, Sixth., no. 1. Elsevier, 2014.

[3]B. Zohuri, *Heat Pipe Design and Technology*. Taylor & Francis Group, 2010.

[4]M. Salem, "A Review : on the Heat Pipe and Its Applications," no. December, 2017.

[5]I. Saad *et al.*, "Heat pipe based systems - Advances and applications," *Energy*, vol. 128, pp. 729–754, 2017.

[6]M. Zheng *et al.*, "Experimental Study of Energy Saving Performances in Chip Cooling by using Heat Sink with Embedded Heat Pipe," *Energy Procedia*, vol. 105, pp. 5160–5165, 2017.

[7]R. S. Melnyk, Y. E. Nikolaenko, Y. S. Alekseik, and V. Y. Kravets, "Heat transfer limitations of heat pipes for a cooling systems of electronic components," *2017 IEEE 1st Ukraine Conference on Electrical and Computer Engineering, UKRCON 2017 - Proceedings*, no. c, pp. 692–695, 2017.

[8]J. Krishna, P. S. Kishore, and A. B. Solomon, "Heat pipe with nano enhanced-PCM for electronic cooling application," *Experimental Thermal and Fluid Science*, vol. 81, pp. 84–92, 2017.

[9]H. Tang, J. Zhao, B. Li, S. Y. Y. Leung, C. C. A. Yuan, and G. Q. Zhang, "Thermal performance of embedded heat pipe in high power density LED streetlight module," in *2014 15th International Conference on Thermal, Mechanical and Multi-Physics Simulation and Experiments in Microelectronics and Microsystems, EuroSimE 2014*, 2014, no. April.

[10]M. Smitka, Z. Kolková, P. Nemec, and M. Malcho, "Impact of the amount of working fluid in loop heat pipe to remove waste heat from electronic component," *EPJ Web of Conferences*, vol. 67, p. 02109, 2014.

[11]S. Aswath, V. H. Netaji Naidu, P. Padmanathan, and Y. Raja Sekhar, "Multiphase numerical analysis of heat pipe with different working fluids for solar applications," *IOP Conference Series: Materials Science and Engineering*, vol. 263, no. 6, pp. 0–6, 2017.

[12]S. Lohrasbi, S. Z. Miry, M. Gorji-Bandpy, and D. D. Ganji, "Performance enhancement of finned heat pipe assisted latent heat thermal energy storage system in the presence of nano-enhanced H2O as phase change material," *International Journal of Hydrogen Energy*, vol. 42, no. 10, pp. 6526–6546, 2017.

[13]J. Kaiser, H. Nasarullah, B. Richard, and S. Abdul, "Comparison between evaporative cooling and a heat pipe assisted thermal loop for a commercial wind tower in hot and dry climatic conditions," *Applied Energy*, vol. 101, pp. 1–16, 2012.

[14]V. V. Vlassov, F. L. De Sousa, and R. R. Riehl, "Design optimization of loop heat pipes with cylindrical evaporator and integral reservoir for space application," *AIP Conference Proceedings*, vol. 969, no. June 2015, pp. 138–145, 2008.

[15]R. R. Riehl and T. Dutra, "Development of an experimental loop heat pipe for application in future space missions," *Applied Thermal Engineering*, vol. 25, no. 1, pp. 101–112, 2005.

[16]V. V. Vlassov and R. R. Riehl, "Modeling of a Loop Heat Pipe for Ground and Space Conditions," *SAE Technical Paper Series*, vol. 1, no. July 2005, 2010.

[17]Charles Hirsch, *Numerical Computation of Internal and External Flows*, vol. 1. 2007.

[18]Oleg Zikanov, *Essential Computational Fluid Dynamics*. Wiley, 2010.

[19]J. D. Anderson, *Computation Fluid Dynamics basic and application*. McGraw-Hill, 1995.

[20]M. Groll, "Heat Pipe Research and Development in Wetern Europe," vol. 9, no. I, pp. 19–66, 1989.

[21]L. Id, "Heat Pipe Principles," *Int. J. Heat Mass Transfer*, vol. 3, pp. 112–125, 1988.

[22] R. Boukhanouf, A. Haddad, M. T. North, and C. Buffone, "Experimental investigation of a flat plate heat pipe performance using IR thermal imaging camera," *Applied Thermal Engineering*, vol. 26, no. 17–18, pp. 2148–2156, 2006.

[23] P. Nemec, A. Caja, and R. Lenhard, "Visualization of heat transport in heat pipes using thermocamera," *Archives of Thermodynamics*, vol. 31, no. 4, pp. 125–132, 2010.

[24] J. C. Wang, "3-D numerical and experimental models for flat and embedded heat pipes applied in high-end VGA card cooling system," *International Communications in Heat and Mass Transfer*, vol. 39, no. 9, pp. 1360–1366, 2012.

[25] A. A. Eidan, S. E. Najim, and J. M. Jalil, "Experimental and numerical investigation of thermosyphone performance in HVAC system applications," *Heat and Mass Transfer*, vol. 52, no. 12, pp. 2879–2893, 2016.

[26] H. Jouhara, B. Fadhl, and L. C. Wrobel, "Three-dimensional CFD simulation of geyser boiling in a two-phase closed thermosyphon," *International Journal of Hydrogen Energy*, vol. 41, no. 37, pp. 16463–16476, 2016.

[27] A. A. Alammar, R. K. Al-Dadah, and S. M. Mahmoud, "Numerical investigation of effect of fill ratio and inclination angle on a thermosiphon heat pipe thermal performance," *Applied Thermal Engineering*, vol. 108, pp. 1055–1065, 2016.

[28] A. A. B. Temimy and A. A. Abdulrasool, "CFD Modelling for flow and heat transfer in a closed Thermosyphon charged with water – A new observation for the two phase interaction," in *Second International Conference on Sustainable Engineering Techniques*, 2019.

[29] T. D. Canonsburg, *ANSYS FLUENT User ' s Guide*. 2018.

[30] T. D. Canonsburg, *ANSYS FLUENT Theory Guide*. 2018.

[31] T. D. Canonsburg, *ANSYS FLUENT Tutorial Guide*. 2018.

[32] M. De Nadra and U. Nacional, "Investigations of the thermal performance of a cylindrical wicked heat pipe," pp. 1–16, 2005.

[33] S. D. De O and R. R. R, "Experimental and Numerical Study of the Thermal Performance of Water-Stainless Steel Heat Pipes Operating in Mid-Level Temperature Experimental and Numerical Study of the Thermal Performance of Water- Stainless Steel Heat Pipes Operating in Mid-Level Tem," no. October, 2018.

[34] S. E. D. Fertahi, T. Bouhal, Y. Agrouaz, T. Kousksou, T. El Rhafiki, and Y. Zeraouli, "Performance optimization of a two-phase closed thermosyphon through CFD numerical simulations," *Applied Thermal Engineering*, vol. 128, pp. 551–563, 2018.

[35] B. Fadhl, L. C. Wrobel, and H. Jouhara, "CFD modelling of a two-phase closed thermosyphon charged with R134a and R404a," *Applied Thermal Engineering*, vol. 78, pp. 482–490, 2015.

[36] B. Fadhl, L. C. Wrobel, and H. Jouhara, "Numerical modelling of the temperature distribution in a two-phase closed thermosyphon," *Applied Thermal Engineering*, vol. 60, no. 1–2, pp. 122–131, 2013.

[37] Y. Kim, D. H. Shin, J. S. Kim, S. M. You, and J. Lee, "Boiling and condensation heat transfer of inclined two-phase closed thermosyphon with various filling ratios," *Applied Thermal Engineering*, vol. 145, pp. 328–342, 2018.

[38] K. Negishi and T. Sawada, "Performance de transfert thermique d'un thermosyphon incline, ferme et diphasique," *International Journal of Heat and Mass Transfer*, vol. 26, no. 8, pp. 1207–1213, 1983.

[39] A. A. Alammar, R. K. Al-Dadah, and S. M. Mahmoud, "Effect of inclination angle and fill ratio on geyser boiling phenomena in a two-phase closed thermosiphon – Experimental investigation," *Energy Conversion and Management*, vol. 156, no. October 2017, pp. 150–166, 2018.

[40] M. Mahdavi, S. Tiari, S. De Schampheleire, and S. Qiu, *Experimental study of the thermal characteristics of a heat pipe*, vol. 93. 2018.

[41] H. Hashimoto and F. Kaminaga, "Heat transfer characteristics in a condenser of closed two-phase thermosyphon: Effect of entrainment on heat transfer deterioration," *Heat Transfer - Asian Research*, vol. 31, no. 3, pp. 212–225, 2002.

[42] B. M. Ziapour and H. Shaker, "Heat transfer characteristics of a two-phase closed thermosyphon using different working fluids," *Heat and Mass Transfer/Waerme- und Stoffuebertragung*, vol. 46, no. 3, pp. 307–314, 2010.

[43] K.-S. Ong and C. Lim, "Performance of Water Filled Thermosyphons Between 30-150Oc," *Frontiers in Heat Pipes*, vol. 6, no. August, 2015.

التمثيل الرياضي والتحقيق التجريبي للمشاهدات الجديدة للتداخل بين الطورين السائل والغازي للحالتين العمودية والمائلة في الأنبوب الحراري بدون الفتيلة ذو التدوير الحراري

علاء عبد الجبار بدن التميمي ¹   عدنان عبد الأمير عبد الرسول ²

١) دائرة التدريب وبحوث الطاقة، وزارة الكهرباء، بغداد- العراق

dralaatemimy@yahoo.com

٢) الهندسة الميكانيكية، الجامعة المستنصرية، بغداد – العراق

adnan_ameer54@yahoo.com

الخلاصة

الأنابيب الحرارية واحدة من الحلول الحديثة لتحرير الطاقة الحرارية من المصادر ذات درجات الحرارة العالية أو للحصول على توزيع منتظم للحرارة في المستودعات السائلة أو الصلبة. ان التداخل بين الطورين السائل والغازي في داخله قد تم فرضه بطريقة تقليدية من قبل الباحثين ولم يتم الكشف عنه بدقة. في هذه الدراسة تم اجراء تقريباً ٤٨٠ حل رياضي وفحص تجريبي مختبري لتأكيد المشاهدات التي نشرناها سابقاً حول انماط الجريان الفضائية غير المنتظمة لكل من الطورين داخل انبوب حراري مصنوع من النحاس وبدون فتيلة يعتمد على التدوير الحراري ومملوء جزئيا بالماء. تم الحصول على النتائج الرياضية من موديل رياضي حسابي ديناميكي انتقالي بالابعاد الثلاثية تم تضمينه مختلف المتغيرات لتقريبه للحالة الواقعية على الرغم من التعقيد في طرق الحسابات وزيادة المدة اللازمة لاكمال التشغيل للمحاكاة الرياضية. ان نسبة التوافق العالية بين نتائج الموديل الرياضي والفحص المختبري لطريقة وقيم التوزيع الحراري تؤكد صحة نتائج الموديل الرياضي. ان المخططات الكنتورية المستحصلة من الموديل الرياضي والخاصة بنمط جريان وتوزيع الطورين داخل الأنبوب الحراري، تبين ان الطورين يجريان بنمط فضائي غير منتظم وغير مستقر وغير مستمر على شكل واحد. كلا الطورين يعانيان من انتقال للحرارة وتغير بالطور مع بعضهما خلال الجريان للاعلى (البخار) او الجريان للاسفل (السائل المتكثف). ازداد الاداء الحراري بنسبة (١٠%+) نتيجة الميلان من الوضع العمودي الى زاوية ٦٠°، ومن ثم انخفض الاداء الحراري بنسبة (١٥%−) بزاوية ١٥° (هذه القيم عند نسبة ملئ ٥٠% وطاقة حرارية مسلطة ٢٠٠ واط). هذا بسبب كون ميلان الانبوب الحراري يؤدي الى تنظيم نمط الجريان الفضائي وتقريبه الى الدوران المنتظم، كما أنه يؤدي الى عدم تجانس عمليتي التبخر والتكثف وبالتالي يؤدي الى انخفاض الاداء الحراري ككل.

الكلمات الدالة: تدوير حراري، ثنائي الطور، أنبوب حراري، اداء حراري، موديل حساب رياضي ديناميكي، نمط جريان، تبخر، تكثف.